Geofísica Internacional (2013) 52-1: 31-42

Original paper

UVB solar radiation climatology for Mexico

Mauro Valdés-Barrón*, Juan Carlos Peláez-Chávez, Roberto Bonifaz-Alfonzo, David Riveros-Rosas, Victor Velasco-Herreºra, Hector Estévez-Pérez

Received: January 31, 2012; accepted: September 04, 2012; published on line: December 14, 2012

Resumen

La medición de la radiación solar ultravioleta B de banda (UVB) debe considerarse como una prioridad debido a las implicaciones de este tipo de radiación en la salud pública en todo el país (población nacional total, 108 millones), pero esto no se lleva a cabo en la actualidad en México. Los sensores instalados, que realizan esta tarea en forma cotidiana, cubren solamente el 0.12% del país. Sin embargo, hay métodos alternativos para estimar la radiación UVB para superar la falta de datos de superficie. El más exitoso de estos se basan en la utilización de satélites de monitoreo ambiental. En el presente trabajo, se construyen los mapas UVB en todo el país mediante una sola medición de satélite diaria de UVB al mediodía en tiempo solar verdadero de 1978-2003. Las mediciones obtenidas del satélite fueron comparadas con mediciones a nivel de superficie desde una estación situada en la Ciudad de México con el fin de validar las primeras. El análisis de espectro wavelet es empleado para este fin. Una estrecha correlación se observa entre los dos conjuntos de datos. Además, no existe correspondencia cualitativa entre la distribución espacial de los datos obtenidos por satélite y la topografía de la superficie. La diferencia resultante durante todo el período mencionado es <2% de la media de la energía acumulada promedio anual.

Palabras clave: radiación solar ultravioleta, UVB, índice ultravioleta, IUV, wavelet

Abstract

The measurement of solar B band Ultraviolet radiation (UVB) should be considered a priority in Mexico due to implications on public health throughout the country (total population, 108 million), but this is not carried out at present. Installed sensors cover only 0.12% of the country. However, there are alternative methods for estimating UVB radiation to overcome the lack of surface data. The most successful of these are based on the use of satellites for environmental monitoring. In the present work, UVB maps are constructed for the entire country using a single, daily satellite measurement of UVB at solar noon from 1978–2003. Satellite-derived values are compared with the ground measurements by a surface station located in Mexico City in order to validate the former. Wavelet spectrum analysis is employed to this end. A close correlation is observed between the two sets of data. Moreover, there is qualitative correspondence between the spatial distribution of the satellite-derived data and the surface topography. The difference resulting throughout the period mentioned is <2% of the average annual cumulative energy.

Key words: solar ultraviolet radiation, UVB, ultraviolet index, wavelet.

M. Valdés-Barrón*
R. Bonifaz-Alfonzo
D. Riveros-Rosas
V. Velasco-Herrera
H. Estévez-Pérez
Instituto de Geofísica
Universidad Nacional Autónoma de México
Ciudad Universitaria
Delegación Coyoacán, 04510
México D.F., México
*Corresponding author: mauro@geofisica.unam.mx

J.C. Peláez-Chávez
Servicio Metereológico de Cuba

Introduction

Solar radiation is the main source of energy on our planet. Different spectral ranges of solar radiation are responsible for triggering several physical and biological processes, which are important to the balance of ecosystems that make up the variety of climates and biodiversity. Specifically, the B band of Ultraviolet solar radiation (UVB) is a small window of the electromagnetic spectrum (with wavelengths ranging from 0.280–0.320 microns) whose photons carry sufficient energy to break the molecules of important components of the atmosphere (ozone, carbon dioxide, nitrogen dioxide, hydrogen peroxide, formaldehyde, nitric acid, etc.). Thus, UVB radiation is linked with the majority of the photochemical processes occurring in the Earth's atmosphere.

The decrease of Ozone (O_3) in the stratosphere at medium and high latitudes has been one of the most serious atmospheric pollution problems in recent decades World Meteorological Organization (WMO, 1994) and is closely related with a severe increase in solar Ultraviolet (UV) radiation in all of the spectral bands (A, B, and C). Because of the great extent of damage to the ozone layer, this phenomenon is manifested on the Earth's surface. The O_3 reduction not only affects the atmospheric composition in terms of concentration or the absence of specific compounds or gases, but also it in general has drastic effects on the health of living beings, including humans. In particular, the amount of UVB radiation reaching the Earth's surface is increased with the decrease in the ozone-layer thickness. This parameter plays an important role in life on the Earth's surface; thus, knowing the UVB spatial and temporal distributions may help in setting up public health programs for the prevention of the short-, mid-, and long-term risks of UVB exposure.

Although in several parts of the world UVB measurements are carried out on a routine basis and are reported (hourly) to the general public (Universität Innsbruck, 2008), (University of Southern Queensland, 2008), due importance has not been afforded to this meteorological parameter in Mexico. There are some isolated cases (point measurements) in which UVB is monitored for research purposes as, for instance, the Universidad Nacional Autónoma de México (UNAM) and the Universidad de Colima (UC). Only the Metropolitan area of Mexico City (MAMC) has a network of UVB sensors, that has been established that produces measurements on a continuous basis and whose results are available to the general public (http://www.sma.df.gob.mx/simat/) (RAMA, 2008).

However, this network has a spatial coverage of merely 2,500 km^2, which is approximately 0.12% of the country. The potential beneficiaries of this activity, therefore, amount to only about 20% of the total national population.

Mexico has a very abrupt orography. Therefore, a meteorological station in many cases cannot be considered representative of the minimum area recommended by the World Meteorological Organization (WMO, 1996); considerable variations in elevation occur within very short distances, causing rapid spatial variation of climatic parameters. Therefore, to ensure continuous and effective monitoring, a surface network would certainly require >1,000 stations. The cost of UVB radiation sensors does not allow the possibility of installing such a large network, and it is also necessary to take additional costs into account, such as preventive and corrective maintenance, as well as annual calibration for the sensors.

Fortunately, there are techniques that can aid us in estimating the levels of B band solar UV radiation at ground level. These techniques range from theoretical radiative transfer models (Gutiérrez-Marco *et al*., 2007), (Kudish *et al*., 2011) to models that utilize meteorological satellite data (Peeters *et al*., 2000), (Ciren and Li, 2003), (Espinar *et al*., 2009), (Janjai *et al*., 2010). The latter is a good alternative, because in the majority of cases it allows evaluation of different meteorological parameters with a single satellite, greatly reducing the aforementioned costs. Moreover, this satellite information is available on the Internet.

In the present work, the results of an assessment of UVB radiation for Mexico are reported. UVB radiation at ground level is evaluated at solar noon. The data used for the evaluation were measured by sensors called Total Ozone Mapping Spectrometers (TOMS), which operated in three different satellites of the National Aeronautics and Space Administration (NASA) from 11/1/1978 to 12/31/2005. These sensors performed nearly constant monitoring of the ozone layer and UVB radiation (Figure 1), generating a highly reliable database for understanding the climatology of the UVB [TOMS, 2011].

Methodology

TOMS are spectrometers that can measure the total amount of ozone in the atmospheric column (from ground level to the top of the atmosphere) under any geographical and atmospheric conditions. Measurements are made in the UV region,

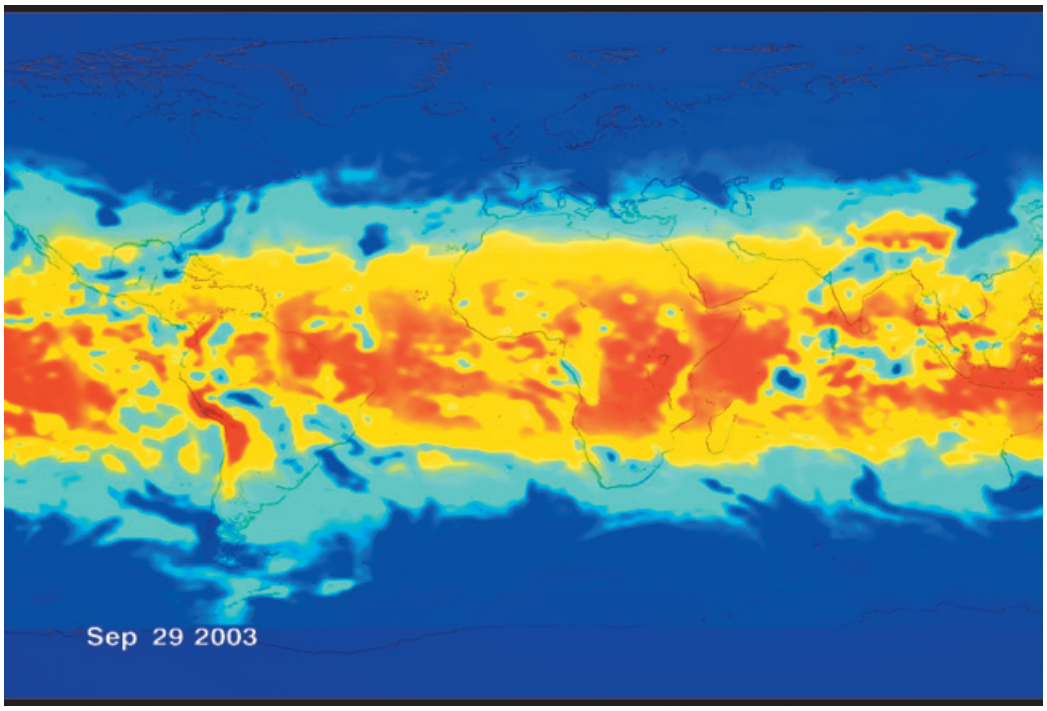

Figure 1. Example of Ultraviolet (UV) image based on data from Total Ozone Mapping Spectrometers (TOMS) during September 29, 2003. The image provides us with a global perspective on the distribution of UV irradiance on the Earth's surface. (Image from Earth Observatory, National Aeronautical and Space Administration, NASA).

where solar radiation is partially absorbed by ozone. They are performed for both incoming and reflected solar radiation. The latter is composed of a part that actually reaches the Earth's surface and is reflected, and of a part that is backscattered into space by the air molecules and clouds. From the measurement of this reflected radiation, UVB at ground level and the thickness of the ozone layer are estimated by means of approximate models (McPeters, 1996).

The instrument has a single, fixed monochromator with exit slits at six near-UV wavelengths (between 308 and 380 nm) and a scanning mirror for sampling backscattered radiation. The accuracy of TOMS was estimated at ±5%, with a spatial resolution of 1° latitude × 1° longitude. These carried out 35 measurements every 8 sec and ground coverage is 50–200 km wide on Earth, depending on the latitude for each meridian. Nearly 200,000 daily measurements cover the surface of the Earth, except for areas near the poles during seasons when the sun remains below the horizon. In practical terms, this technology allows having, in the case of UVB, a single, daily data point for 12:00 hrs TST (True Solar Time) (McPeters, 1996), (Herman, 1996), (McPeters, 1998).

Data Source

The information can be obtained in the NASA web server for TOMS (http://toms.gsfc.nasa.gov/ery_uv/euv_v8.html). It corresponds to global coverage on daily arrays that are ordered in latitudinal groups that range from 89.5° South to 89.5° North. Longitude is covered from 179.5° West to 179.5° East. The readings are expressed in milliWatts per square meter (mW/m²), and as mentioned previously, each value corresponds to a single data point at noon TST. Each reading is expressed with a group of three digits, for example, 245. The first corresponds to the exponent for each datum in scientific notation, and the last two digits comprise the reading divided by 10. For example, 245 correspond to the 4.5 × 10² mW/m² reading.

From the overall global matrix, we selected the data bound between 84° and 120° West, and 10° and 36º North, which by far contains the entire territory of Mexico. These limits are sufficiently far from the true geographical extension of the country for the interpolation of climatological values to be free of edge effects; i.e., there is no need to be concerned with distortions caused near the points on the edges

of the array. Thus, after using the data to obtain the desired contours, the area-of-interest is cut by about 3° of latitude and 3° of longitude on each end.

First, the TOMS files were transferred from the data server, one file for each day since 1978 and up to 2003. From this information, daily files for the selected coordinates were obtained. The selected data were employed to generate matrices of monthly and annual averages, and also seasonal matrices.

Using a Geographic Information System (GIS), matrices with the average monthly points were incorporated and interpolated with the Kriging's method to obtain an array, with the interpolated values in color gradation, in order to differentiate intensities and the contours for each month. Furthermore, a digital elevation model was included and the state boundaries in a Lambert Conical Conformal projection.

After obtaining the maps, measurements reported by surface stations were used to validate the information obtained by this procedure. The available surface stations comprise the Solar Radiation Observatory (ORS) of the Instituto de Geofísica (IGeof) of the Universidad Nacional Autónoma de México (UNAM) and the stations in the Red Automática de Monitoreo Atmosférico (RAMA) of the Mexico City Government. Both systems generate highly reliable information because each station meets WMO requirements. However, we decided to use the data from ORS (19º 20′ 01′′ ‹North Latitude, 99º 10′ 54′′ West Longitude at 2,268 m above sea level) because this is considered by WMO as a Regional Centre for Solar Radiation in the IV Region (AR-IV).

To make this comparison, we used a Solar Light sensor, model 501a, serial number 2010. This sensor works in a spectral window from 0.280–0.320 μm (Solar Light, 1991).

As discussed previously, information from the satellite observations is registered once a day, at true solar noon, while the surface data are measured every minute. Therefore, the surface measurements used for comparison correspond to those at 11:59, 12:00, and 12:01 TST, which were averaged in order to compensate for possible delays or advances of a few seconds with respect to the satellite observation.

Wavelet analysis

To analyze local variations of power spectrum within a single non-stationary time series at multiple periodicities, such as UVB surface data and satellite data, the Morlet Wavelet is applied here because it provides higher resolution in the periodicity and because being a complex function allows us to analyze the evolution of periodicities in the time-space and to calculate the phase between two time series (Soon *et al.* 2011).

The Morlet wavelet consists of a complex exponential function modulated by a Gaussian wavelet and is defined as:

$$e^{i\omega_o t/s} e^{-t^2/(2s^2)}, \qquad (1)$$

where t is the time with s = *period* as the wavelet scale and ω_0 is a non-dimensional frequency. Here, $\omega_0 = 6$ to satisfy the admissibility condition (Farge, 1992).

The cone of influence (COI) is the region of the wavelet spectrum outside which the edge effects become important (Torrence and Compo, 1998).

Wavelet Power Spectral Density (WPSD) is calculated for each parameter; the black thin lines in Figures 2, 3 and 4 marks the 95% confidence interval or boundaries of COI.

We use the inverse wavelet transform to obtain the decomposition of a signal and can be obtained from a time-scale filter (Mendoza and Velasco, 2011). Inverse wavelet transform is defined (Torrence and Compo, 1998) as:

$$X_n = \frac{\delta_j \delta_t^{1/2}}{C_\delta \psi_o(0)} \sum_{j=0}^{J} \frac{\mathrm{Re}\left\{W_n\left(s_j\right)\right\}}{s_j^{1/2}}, \qquad (2)$$

where δ_j is the factor for scale averaging, C_δ is a constant (δ_j = 0.6 and C_δ = 0.776, for Morlet wavelet), and ψ_0 removes the energy scaling.

The cross wavelet $W_k^{X_1X_2}(\psi)$ (XWT) was used which measures the common power spectrum between the input (X_1) and output (X_2) in physics system and is defined as (Torrence and Compo, 1998):

$$W_n^{X_1,X_2} = W_n^{X_1} W_n^{X_2}, \qquad (3)$$

where (*) denotes complex conjugation, ($W_n^{X_1}$) and ($W_n^{X_2}$) is the wavelet transforms (WT) of the time series X_1 and X_2

The arrows in the cross-wavelet spectra show the mean relative phase between the X_1 (input) and X_2 (output) series in time-frequency space: arrows at 0° (pointing to the right) indicate that both time series are perfectly positively correlated (in phase) and arrows at 180° (pointing to the left) indicate that they

are perfectly negatively correlated (180° anti-phase). It is important to point out that these two cases imply a linear relationship between the considered phenomena. Non-horizontal arrows indicate an out of phase situation, meaning that the two studied phenomena have a more complex non-linear relationship.

On the left panels of Figures 2, 3, and 4, the wavelet *global spectra* are shown, which is an average power of each periodicity in both the wavelet and the cross spectra.

The significance level of the global wavelet spectra is indicated by the dashed curves; they refer to the power of the red noise level at the 95% confidence level that increases with decreasing frequency (Grinsted *et al.* 2004).

Results and Discussion

The results of the previously described procedure are presented in Figures 2–4, in which the global wavelet spectrum is shown as a function of time.

In Figure 2, it can be observed that the global wavelet spectrum (panel C) of the surface data shows a prominent annual periodicity, with a 95% confidence interval (95% CI) defined by the red noise (red dotted line). As we can also observe (panel B), the Morlet wavelet is present throughout all time intervals (framed by a black line). In addition to the 1-year period, half-year periodicity is also present in the overall wavelet spectrum throughout the time interval (1997–2003). Additionally, there are periodicities on the order of a few days that can be observed, especially around the maxima of the time series of surface data shown in panel (A).

It should be noted that these periodicities of a few days (66, 35, 20, 9, 4 and 2) are located around the descending part of the annual maximum. The chart also provides information on the behavior of UVB intensity at the surface. As can be observed, the years 1998 and 2001 were the most intense over the period of study.

Similarly to the surface data, the global wavelet spectrum (panel C) of the satellite data (Figure 3) shows a prominent annual periodicity, with 95% reliability; as one may observe, the Morlet wavelet (panel B) is present throughout the time interval (1997–2003). There is also a half-year periodicity that is present throughout the time series, but with less intensity than in the surface data. In addition, there are periodicities of 2, 10, 15, 33, and 74 days around the maximum of the time series of surface data. However, in the satellite data, these periodicities are more spread out over the maximum.

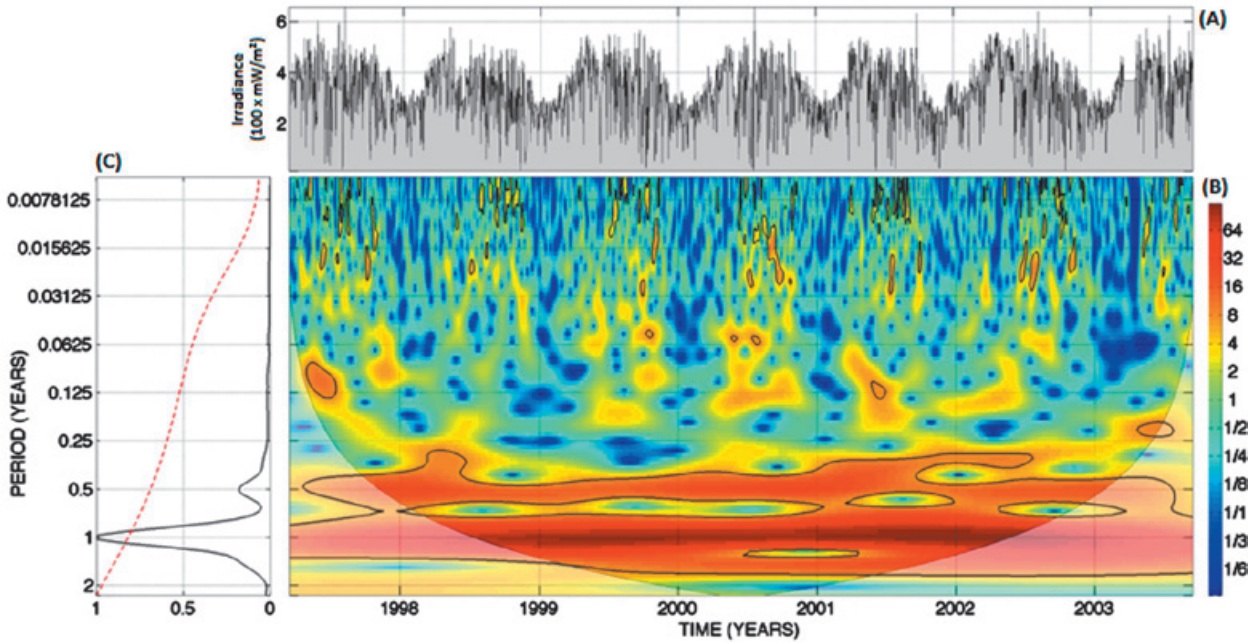

Figure 2. Wavelet spectrum for surface data. Upper graph (panel A), time series; lower right (panel B), wavelet power spectra; lower left (panel C), global wavelet spectrum.

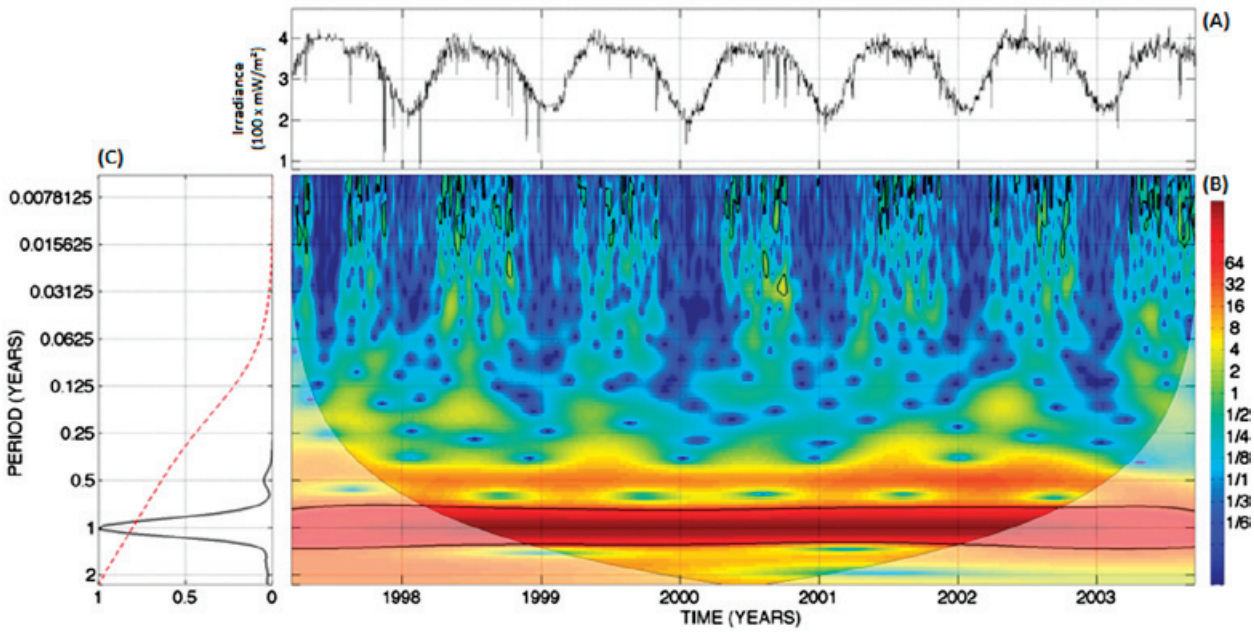

Figure 3. Wavelet spectrum for satellite data: (panel A), time series; lower right (panel B), wavelet power spectra; lower left (panel C), wavelet global spectrum.

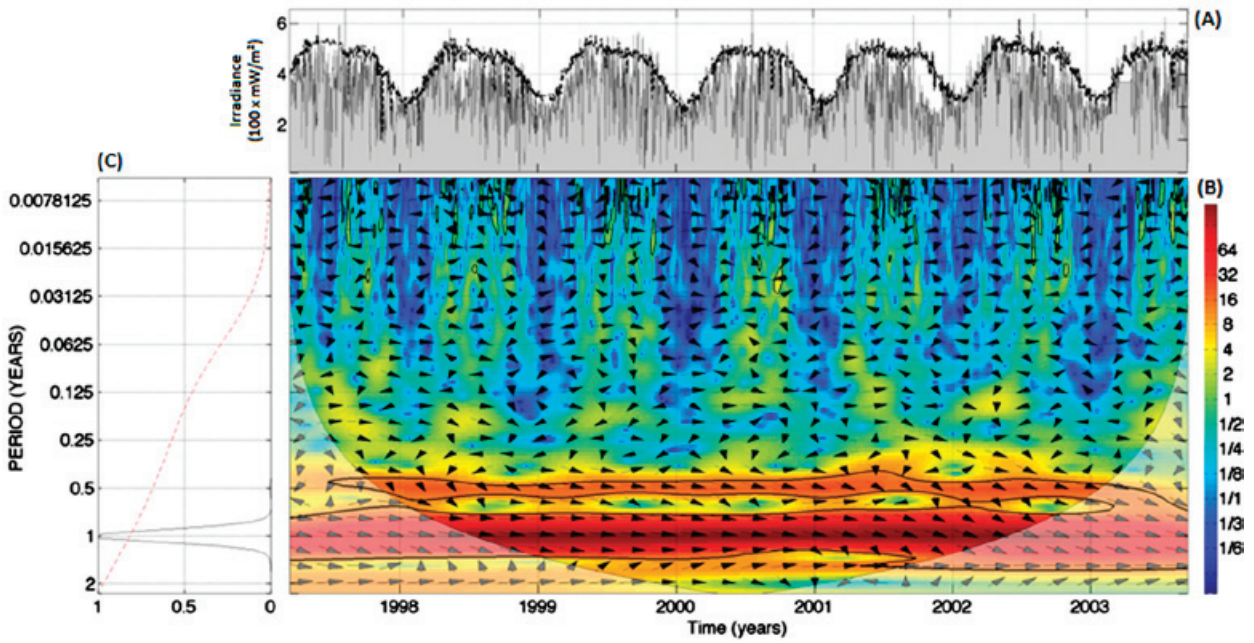

Figure 4. Cross-wavelet spectrum of surface data with satellite data. Upper graph (panel A), time series; lower right (panel B), wavelet power spectra, shown in color and a relative phase difference is indicated by the arrows.; lower left (panel C), wavelet global spectrum.

The wavelet global spectrum (panel C) from surface data and satellite data (Figure 4) shows that the common periodicity, both in phase and maximum value, is annual, with 95% reliability, with the cross-wavelet (panel B) present throughout the time interval (1997–2003). There are also other periodicities in common with <95% reliability that have a frequency of about one half year and that are also present throughout the whole period. The periodicities of 2, 9, 20, 35, and

66 days are present mainly around the maximum of the time series of surface and satellite data. The arrows show a phase lag between surface and satellite data because the former are local and point measurements, while the latter are global volumetric; while the surface data are measured at a given point on the surface of the Earth, the satellite data represents an average of the processes of extinction of UVB radiation throughout the atmosphere within an area of about 1° latitude × 1° longitude and where weather conditions can change locally. Thus, periodicities on the order of a few days are not synchronized between the two series. We can observe that for half-year periodicities under the relationship is nonlinear and complex, because the arrows indicating the phase in the two time series, shows random orientation, while for periodicities greater than half-year, the arrows are oriented from left to right indicating a linear behavior.

In panel C, values of the "classical" correlation coefficient of the information derived from surface and satellite measurements are presented. This coefficient has low values, indicating that there is a non-linear relationship between the two. This makes the advantage of the cross-wavelet (Figure 4) evident: it does not matter whether the two data sets are linearly dependent or not because the local correlation coefficient is computed independently for each of the periodicities involved; therefore, we have a high coefficient in the periodicities (few days, 6 months, and annual).

The results of wavelet analysis, is used to filter the data (for a comparison) and improve the correlation between surface data and satellite measurements. Figure 5(a) shows the comparison between these data and Figure 5(b) shows a remarkable improvement of the correlation coefficient.

We use the inverse wavelet transform (eq. 2) to obtain the time series > 1 years. Were filtered data that correspond to periodicities less than 1 year and they were identified through wavelet analysis. The correlation coefficient is significantly better after filtering the data. Before filtering the correlation coefficient was 0.3758, after filtering the correlation coefficient was 0.7462.

As an example of the results, we present the average monthly maps of one month of the winter season (Figure 6) and one month of the summer season (1978-2003) (Figure 7), where it can be seen the spatial distribution of UVB throughout the country (January and August). The green point on figures indicates the position of surface sensor in Mexico City.

During the winter, when the Sun declination reaches its maximum negative value, the solar radiation reaches the surface of the Earth with greater inclination significantly reducing the energy per unit area, so that the distribution in surface UVB predominantly responds to latitudinal pattern throughout the country, which is only modified by major topographic features (Volcanic Belt, Sierra Madre Occidental, Sierra Madre Oriental and Sierra Madre del Sur).

For the summer months the shape of the isolines is completely different, as a predominantly latitudinal distribution, going to concentrate the maximum values in the upper parts of the main topographical features (Volcanic Belt, Sierra Madre Occidental, Sierra Madre del Sur and Sierra de Baja California) with a gradient which tends to decrease to the sea level. This is because during the months around the summer solstice, the sun declination angle is positive and the sun's path at noon is near to the zenith. For this reason the sun's irradiation is greater, the solar radiation interacts less with the Earth's atmosphere, so the processes of extinction of solar radiation are reduced.

Finally, in Figure 8, we can see the different values of monthly average UVB for three sites located at similar latitude: Manzanillo City, Colima. (19° 03' N, 104° 18'W, 5 m AMSL), Tlamacas Station on the northern flank of the volcano Popocatépetl (19° 03' N, 98° 37' W, 3867 m AMSL) and Boca del Río, Veracruz (19° 03' N, 95° 59' W, 14 m AMSL) but at different altitudes (Figure 9).

Values corresponding to the station Tlamacas, always remains above the other two sites, due basically to the altitude. While less atmosphere through solar radiation, fewer extinguishing processes act on it and the amount of energy per unit area will be greater. For the other two sites (Manzanillo, Col. and Boca del Río, Veracruz), the radiation must cross more atmosphere and the extinction processes will be grater. The difference between the last two curves, is primarily due to climatic factors, among which, topography, (Boca del Río is located on a very wide coastal plain, while in Manzanillo, coastal plain barely exists); Boca del Río is much more exposed to the phenomena of "North" in winter. In summer the effects of tropical storms and tropical cyclones are more frequently in Boca del Rio in the Gulf of Mexico than in Manzanillo in the Pacific area.

An important point to note is that apparently there are only three periods in the behavior of the UVB at the surface, the first of January to March where the radiation simply increases to

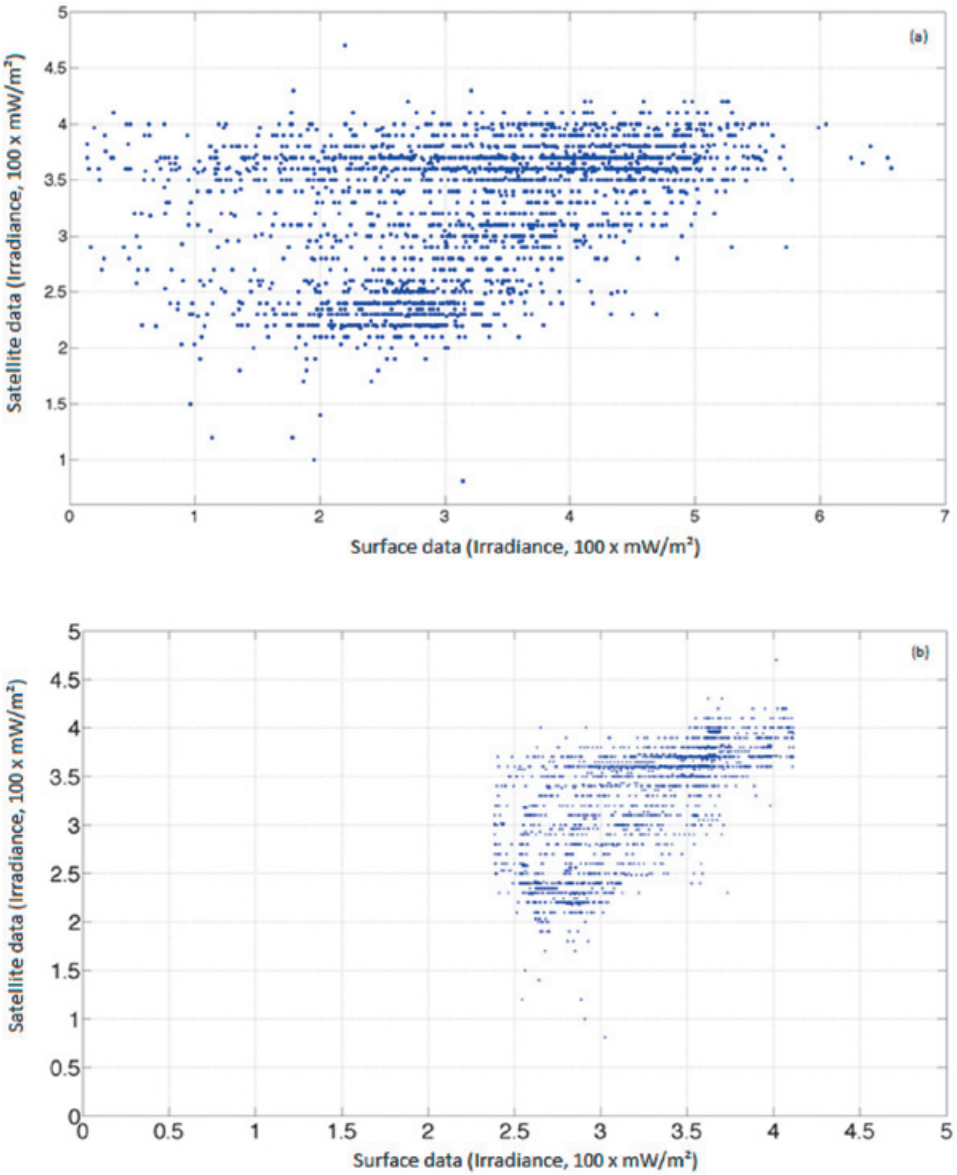

Figure 5. Comparison between surface and satellite data, upper graph (a) before filtering data, lower graph (b) after filtering data.

reach its peak in the month of March. After a period of semi-stability which runs from April to August or September where, although it has a tendency decrease, at the end of this period is stabilized. And the third and final stage, which is a clear decrease in solar irradiance during the months of October to December where in the last month has again reached its minimum values.

Finally it is important to mention that the main factors that determine the spatiotemporal distribution of solar radiation on the surface, are cloudiness and topography, and the results presented here, are influenced by these two factors, the relative distribution of UVB on the surface to the whole country can be considered highly reliable. But we must not forget one important limitation of this work, there was only a single reference point (Mexico City) to validate the UVB satellite measurements, so we cannot generalize concerning the validity of measurements on each point for the entire country, because it does not have sufficient reference points on this surface.

During the majority of autumn and winter months (January, February, March, November, and December), when solar declination is negative and the Sun's rays reach the surface in more inclined fashion, the distribution of UVB is nearly latitudinal. There are also two transition months (April and October) between this "winter" behavior and what might be called "summer", where the latitudinal distribution

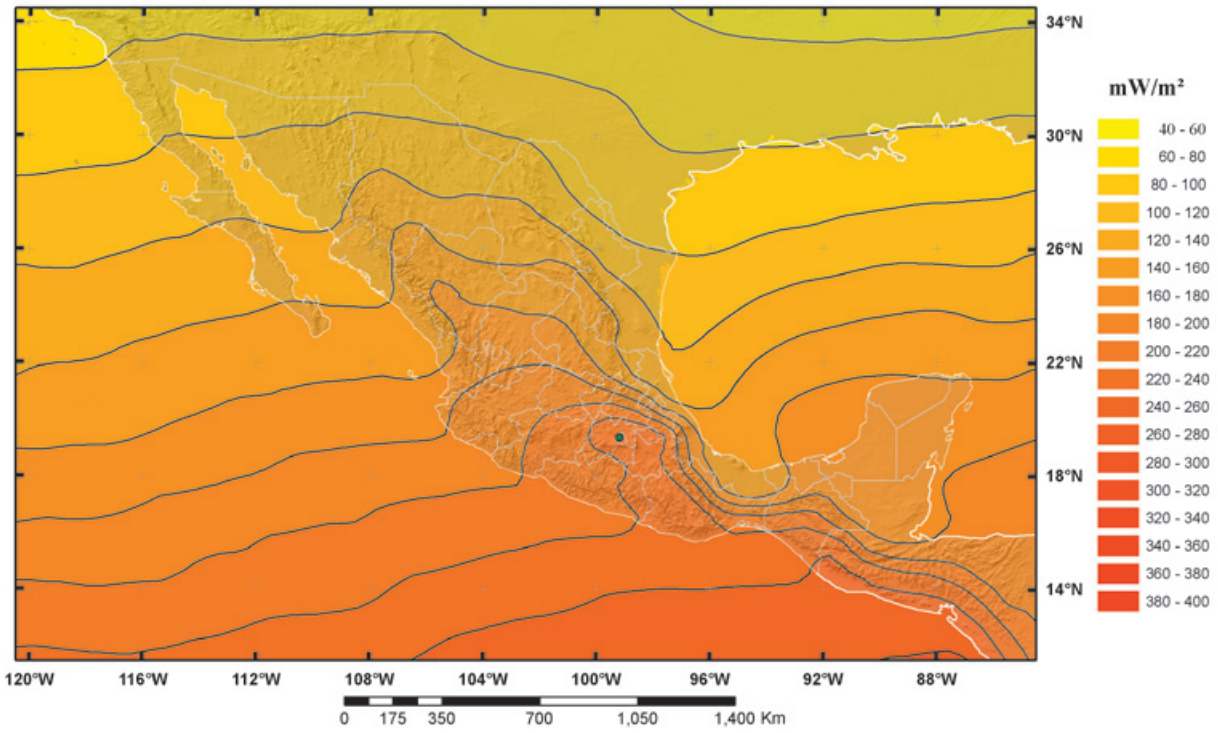

Figure 6. UVB solar Radiation. January monthly mean average (1978–2003).

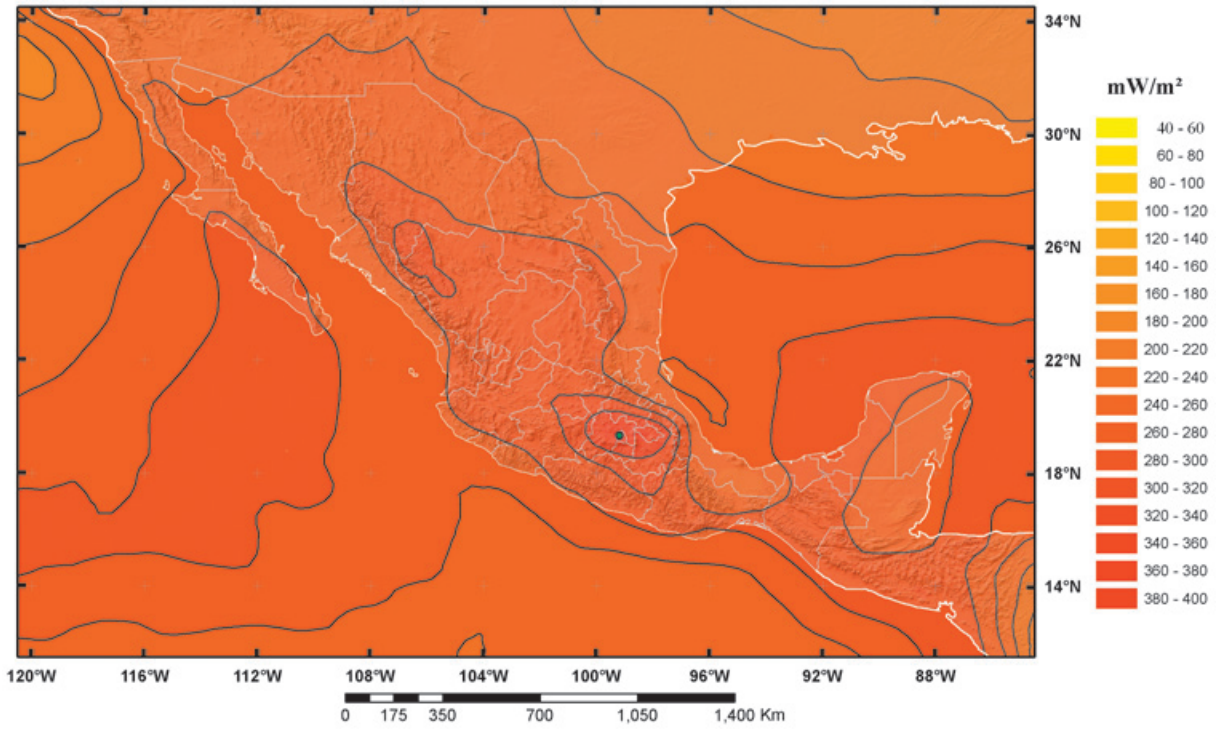

Figure 7. UVB solar Radiation. August monthly mean average (1978–2003).

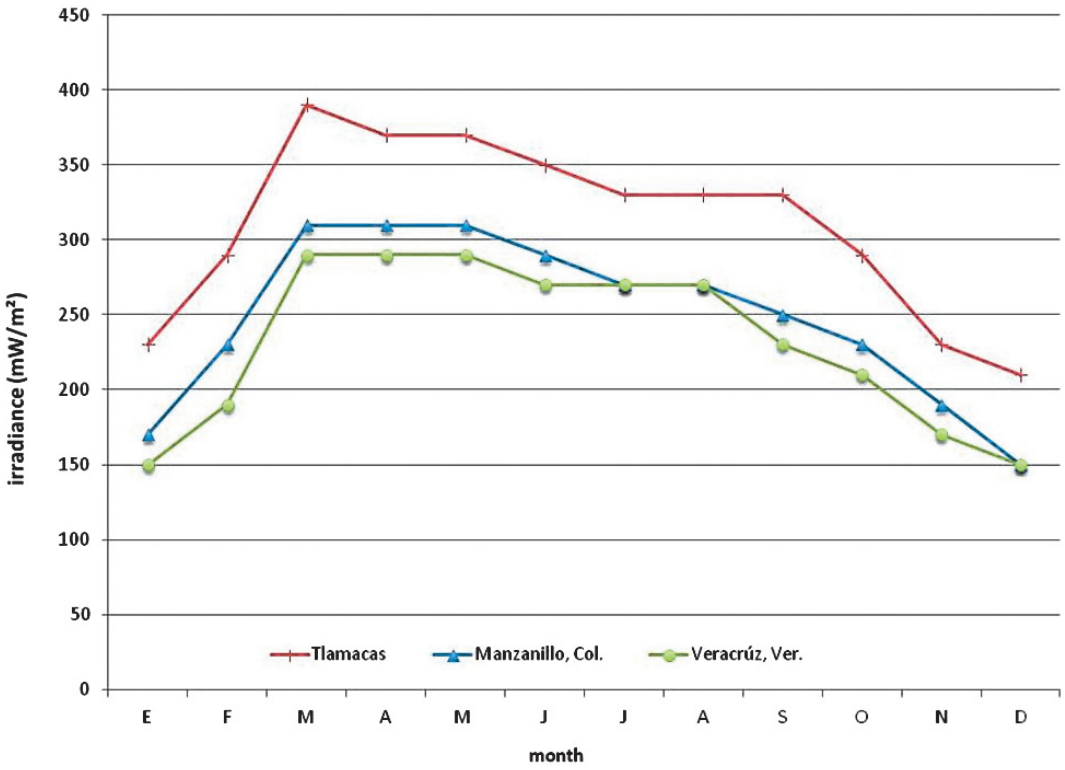

Figure 8. Monthly average UVB for three sites located at similar latitude and different altitude.

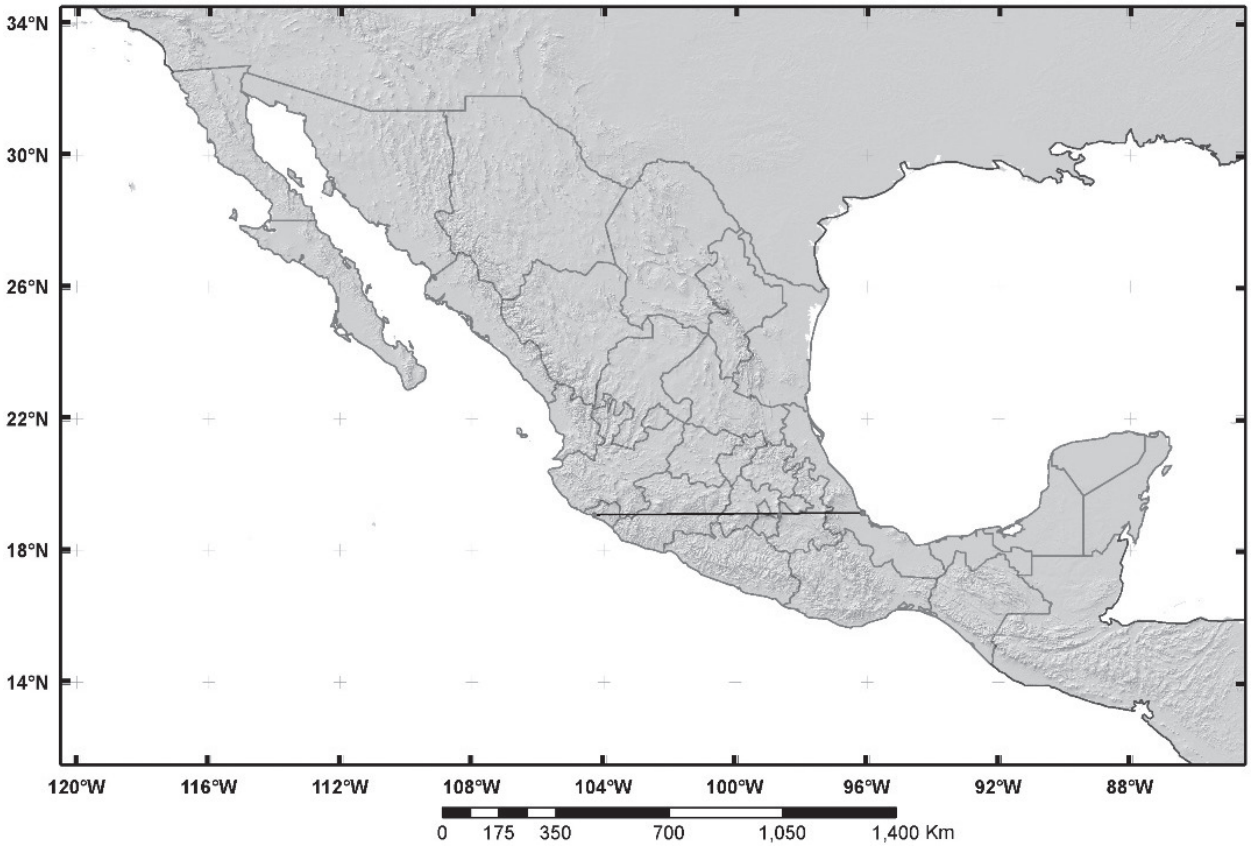

Figure 9. Transect for three sites at similar latitude (red dots). Manzanillo (left), Tlamacas (middle), Veracruz (right).

of UVB seems to disappear. The latter occurs because solar declination is positive and the rays reach the surface in a nearly vertical direction at this time of the year, reducing the optical mass of atmosphere crossed by radiation. The highest values for UVB radiation are found in the highest parts of the major topographical features of the country (*Cinturón Volcánico Transversal, Sierra Madre Occidental, Sierra Madre del Sur,* and even in the *Sierra de Baja California*).

The previously mentioned behavior may be considered as "expected", due primarily to that during the winter months, the Sun's rays reach the surface with such an inclination that higher values were close to Ecuador and smaller values are oriented toward the North Pole. There is also a small deformity in latitudinal distribution due to the *Cinturón Volcánico Transversal* and the *Sierra Madre Occidental*, major topographic features of the country, and this deformity responds to the presence of higher values than those found for the remainder of the national territory. It is necessary to recall that solar radiation undergoes extinction processes such as absorption, reflection, and scattering, and extinction grows while the optical path increases; thus, higher values are always found at higher altitudes.

This extinction process can be identified in the "summer" months, when the angle of incidence for solar radiation is close to the vertical direction over the surface of Mexico. Therefore, distribution of UVB values has greater intensity in the higher parts of Mexico, while the latitudinal distribution that characterizes the winter months is completely lost.

It is noteworthy that these maps were obtained with observations at 12:00 hrs TST, which means that they were carried out when the sun is at its highest position. In other words, the data correspond to the maximum intensity of radiation that can reach the surface on a given day; therefore, the expected maximum radiation is depicted in the maps.

Conclusions

The use of satellites for the evaluation of natural resources or environmental monitoring, specifically in the case of UVB, are of vital importance as they provide an affordable option as opposed to a network of sensors that are sufficiently dense to carry out monitoring on this scale.

While the behavior of UVB radiation can be known through models that describe radiation transfer through the atmosphere, it had never been possible to carry out such a description for the whole country, due in part to the lack of detailed information on the local composition of the atmosphere. This work represents, to our knowledge, the first assessment of the spatial and temporal distribution of solar UVB radiation for Mexico.

Satellite measurements of UVB obtained at the reference point at the ORS in Mexico City showed good correlation with surface measurements, which ensures the reliability of the satellite data at that point. Moreover, spatial and temporal distribution throughout the year is consistent with the behavior that one might expect from the geographical variation of altitude and latitude of the studied area. Therefore, the use of satellite sensors appears to be suitable for the country. This may help to identify areas with the highest values of UVB radiation, either for application in health policy and prevention of UVB overexposure, or for applications in renewable energy using this type of radiation. It would be desirable to have more ground stations for comparison for more rigorous assessment of the validity of the method.

Acknowledgments

The authors thank Mr. Ismael Velázquez-Orozco for his support in the management of computer equipment, Mr. Ernesto Jiménez de la Cuesta for his support for data processing of UVB radiation, and Dr. Camilo Arancibia-Bulnes for his comments on the manuscript.

Bibliography

Ciren P., Li Z., 2003, Long-term global Earth surface ultraviolet radiation exposure derived from ISCCP and TOMS satellite measurements, *Agricultural and Forest Meteorology*, 1-4, 120, 51-68 p., ISSN 0168-1923.

Espinar B., Ramírez L., Drews A., Georg Beyer V., Zarzalejo L.F., Polo J., Martín L., 2009, Analysis of different comparison parameters applied to solar radiation data from satellite and German radiometric stations, *Solar Energy*, 1, 83, 118-125 pp.

Farge M., Goirand E., Meyer Y., Pascal F., Wickerhauser M.V., 1992, Improved predictability of two-dimensional turbulent flows using wavelet packet compression, Fluid Dynamics Research, 10, 4-6, 229-250.

Grinsted A., Moore J.C., Jevrejeva S., 2004, Application of the cross wavelet transform and wavelet coherence to geophysical time series, Nonlinear Processes Geophys., 11, 5-6, pp 561–566.

Gutiérrez-Marco E., Hernández E., Camacho J.L., Labajo A., 2007, Analysis of UVB values in the centre of the Iberian Peninsula, Atmospheric Research, 84, 4, pp 345-352.

Herman J.R., Bhartia P.K., Krueger A.J., McPeters R.D., Wellemeyer C.G., Seftor C.J., Jaross G., Torres O., Labow G., Byerly W., Taylor S.L., Swissler T., Cebula R.P., Gu X.Y., 1996, Meteor–3 Total Ozone Mapping Spectrometer (TOMS) Data Products User's Guide, NASA Reference Publication 1393. National Aeronautics and Space Administration, Washington, DC.

Hernández Ordóñez A.E., 2000, Climatología de la Radiación Solar Ultravioleta Banda "B" en la ZMCM, Tesis de Licenciatura, Facultad de Filosofía y Letras, Universidad Nacional Autónoma de México.

Janjai S., Buntung S., Wattan R., Masiri I., 2010, Mapping solar ultraviolet radiation from satellite data in a tropical environment, Remote Sensing of Environment, 114, 3, pp 682-691.

Kudish A.I., Evseev E.G., 2011, The analysis of solar UVB radiation as a function of solar global radiation, ozone layer thickness and aerosol optical density, Renewable Energy, 36, 6, pp 1854-1860.

McPeters, R.D., Bhartia P.K., Krueger A.J., Herman J.R., Schlesinger B.M., Wellemeyer C.G., Seftor C.J. , Jaross G., Taylor S.L., Swissler T., Torres O., Labow G., Byerly W., Cebula R.P., 1996, Nimbus-7 Total Ozone Mapping Spectrometer (TOMS) Data Products User's Guide. NASA Reference Publication 1384. National Aeronautics and Space Administration, Washington, DC.

McPeters, R D., Bhartia P K., Krueger A.J., Herman J.R., Wellemeyer C.G., Seftor C.J., Jaross G., Torres O., Moy L., Labow G., Byerly W., Taylor S.L., Swissler T. and Cebula R.P., 1998, Earth Probe Total Ozone Mapping Spectrometer (TOMS) Data Products User's Guide. NASA Reference Publication 206895, National Aeronautics and Space Administration, Washington, DC.

Medizinische Universität Innsbruck, Sektion für Biomedizinische Physik, 2008, http://www.uv-index.at/.

Mendoza B., Velasco Herrera V.M., 2011, *Solar Physics*, 271, 169-182 p.

Observatorio de Radiación Solar, 2008, http://www.geofisica.unam.mx/ors/ors-red.html Instituto de Geofísica, Universidad Nacional Autónoma de México.

Organización Meteorológica Mundial (WMO), 1996, Guía de Instrumentación y Observaciones Meteorológicas, Geneva, Switzerland.

Organización Meteorológica Mundial (WMO), 1994, The International Programme on Chemical Safety (IPCS), Environmental health criteria, 160, Geneva, Switzerland.

Peeters P., Müller J.-F., Simon P.C., Gillotay D., Celarier E.A., Herman J.R., 2000, Monitoring surface UV-B irradiance from space using GOME; comparisons with ground-based measurements, Advances in Space Research, 26, 12, pp 1941-1947.

Sistema de Monitoreo Atmosférico de la Ciudad de México, 2008, http://www.sma.df.gob.mx/simat/.

Solar Light Co., Inc., 1991, *UV- Biometer, User's Manual 501*, Solar Light Co. Inc.

Soon W., Dutta K., Legates D.R., Velasco V., Zhang W.J., 2011, Variation in surface air temperature of China during the 20th century, Journal of Atmospheric and Solar-Terrestrial Physics, 73, pp 2331-2344.

Torrence C., Compo G.P., 1998, *A Practical Guide to Wavelet Analysis*. Bull. Amer. Meteor. Soc., 79, pp 61–78.

University of Southern Queensland, Toowoomba, Australia, 2008, http://www.usq.edu.au/faculty/science/depts/biophysci/weather/biometer/biometer1.htm.